Solar Energy 297 (2025) 113542

Contents lists available at ScienceDirect

Solar Energy

journal homepage: www.elsevier.com/locate/solener

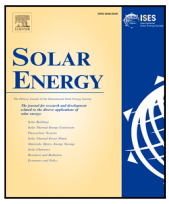

A simple method to estimate the degraded photovoltaic modules from the string open-circuit voltage in solar pumping systems

José Antonio Moreno [a], Rafael Muñoz [b,*]

[a] Department of Structural Mechanics and Hydraulic Engineering, University of Granada, ETS Ing. Caminos. C/ Dr. Severo Ochoa s/n, Granada, 18001, Spain
[b] Department of Civil Engineering, University of Granada, ETS Ing. Caminos. C/ Dr. Severo Ochoa s/n, Granada, 18001, Spain

ARTICLE INFO

Keywords:
Photovoltaic
Potential-induced degradation
PID
In-field
Open-circuit voltage
String voltage
Solar pumping

ABSTRACT

Four regression methods are presented to estimate the number of highly degraded solar panels per string affected by severe potential-induced degradation (PID) from the open-circuit voltage measurement of the string.

Three case-study plants, initially affected by PID and evolving into additional problems, are shown. In the tenth year of operation, the plants' energy production dropped 67.58%, 47.22% and 32.06% below the average annual production in the four first years. The plants are on the roof of agro-industrial facilities, supply power to irrigation pumping systems, and are subjected to high temperatures and humidity.

The proposed method solves a heat stress health safety problem, prevents water supply failures, and estimates the size of repowering purchases. Days with very high temperatures are the best times to detect PID in the field but they represent a safety problem for the maintenance workforce in very hot areas. The method is fast and it is not necessary to reach the roof. The methods were also designed and used to estimate the number of degraded panels to be replaced, proceeding to purchase orders based on these estimates. Significant adjusted R^2 values between 0.64 and 0.82 were obtained depending on the regression method used.

1. Introduction

The operation and maintenance of photovoltaic (PV) plants require different simulation tools and data collection systems to know the state of the plant and predict its behavior, such as predictions of power output [1–4] or fault diagnoses [4–7]. These methods can be online or offline, including in the latter manual measurements at certain times with more limited but focused capabilities.

Faults can be divided into module level faults, PV array level and electrical faults . Electrical faults [8] refer to those in the AC side, in the inverter, battery banks if any and MPPTs. Module level faults [9,10] are related to physical issues like delamination, discoloration, corrosion, busbar or ribbon disconnections, snailtracks, cell cracking, effects of aging, PID and failures related to environmental aspects, like shadowing, snow covering or dust accumulation. Other authors categorize failure focusing on its influence on the parameters of the electrical circuit of the cell/module, and deal with shunts [11] if the shunt resistance lowers and with defects that increase the serial resistance [12]. Most faults caused by degradation affect both [9].

The majority of shunts are originated in the manufacturing process rather than by defects in material crystallography [11]. Methods for detection in modules are visual inspection, infrared and electroluminiscence imaging, ultrasonic testing, insulation resistance, I-V curve analysis or parameter extraction by modeling the electrical equivalent circuit. Statistical analysis, signal processing, machine learning and deep learning algorithms are being apply to empower these methods for identification, classification and prediction. The increasing complexity of the diagnostic systems to enhance fault discrimination [5] will require measurements at the module or at the cell level [13,14].

The PV array faults [8], are related to electrical interconnections; connection to earth, line-to-line faults, open-circuit fault of a string, bridging, bypass diode, junction box connections. Measurements at the PV array level reduce the fault detection capacity [15,16]. PV array power, currents and voltages (including I-V curves) related to irradiation readings are common in this scale, and procedures combine falling down to the string level when an anomaly is detected and finally to the module level [17].

While trends are necessarily moving toward the presence of increasingly complex control systems, simplicity and adequacy of data collection in accordance with the scope must be considered, as well as the size of the plant. The global cost of the control system is another important variable [18,19], and many costs are not accounted for in terms of sustainability [20]. Efforts in cost-effective detection with the minimum sensors, have recently arisen, like [21], proposing voltage

* Corresponding author.
E-mail addresses: jamoreno@ugr.es (J.A. Moreno), rmb@ugr.es (R. Muñoz).

https://doi.org/10.1016/j.solener.2025.113542
Received 9 July 2024; Received in revised form 20 March 2025; Accepted 18 April 2025
Available online 22 May 2025

measurements between pairs of neighboring strings added to the PV array general readings (power, voltages and currents and irradiation). The method senses at PV array and string levels, allowing the location of the failing string, and gives an approximation of the number of the module in the string that is failing, by simple comparison between the expected and real operating voltages of the string.

The presence and complexity of the control system is proportional to the size of the plant and there are many medium and small plants that rely on manual simple methods.

This paper is mainly concerned with the detection of failures that affect the Voc at the string level, to go down to the module level, just to predict the number of failing modules in the string. An example of such a condition can be potential-induced degradation (PID), the evolution of which can lead to major failures also expressed in Voc degradation. So, the core motivation that drives this work is twofold with equivalent importance; the first one is related to the reliability of supply in the long-term and the decision to repower the plants, suitably sizing the purchases of new panels, and the second one with the human factor of maintenance operators in terms of health-security, both framed in the commented simplicity of data.

The PV plants considered in this study are located in an area of Spain with severe incidence of potential-induced degradation (PID) of shunting type (PIDs), which triggers other failures expressed in Voc degradation. The main power loss of the modules that present such degradation occurs during the part of the year with higher temperatures. Maximum ambient temperatures of 40–42 °C are common in this area in summer. In addition, they are installed on the roof of agro-industrial plants, where the thermal stress suffered by maintenance operators [22,23] is multiplied by the radiation heat received from the surrounding elements. The subjective thermal feeling can exceed 50 °C, a situation that multiplies the risk of thermal shock. These are the hard conditions in the best moment of the year to detect whether the module presents degradation. On the other hand, most low- and medium-sized plants in the area do not have more than the basic measurement and control infrastructure, which does not allow going too deep into the fault detection capacity.

The need arises for maintenance operators to have a quick method to estimate the number of modules with a certain thershold of degradation from a simple and quick measurement. In this case, it is the Voc of the string, which can be performed in the protection and control cabinet. The operation process is greatly accelerated and avoids having to go up to the roof to perform the measurements module by module for a long time under dangerous thermal stress conditions. Once the measurements have been taken, the result obtained in the estimation process can be used to order new modules and proceed with the repowering of the plant, or for any other purpose.

The paper is organized as follows. Section 2 reviews the possible causes of Voc drop and deepens on the aspects of PID that are relevant to this paper. Section 3 describes the methodology, including the description and historical performance of the three solar plants and the laboratory tests. The models used to estimate the number of degraded modules to be replaced are explained in Section 4. Section 5 shows the results of the lab tests and the models. Finally, Section 6 is the discussion and Section 7 for conclusions.

2. Causes of open-circuit voltage drop

A perspective that helps to understand a deficit in Voc is the equivalent circuit of the cell (two-diode model). In open-circuit condition there is no external current, so there is no voltage drop in the series resistance (Rs). Then, drops in Voc must come from the processes at the pn-junction under illumination (photocurrent generation), drops in the shunt resistance and excesses in the recombination process (non-ohmic shunts).

All defects that avoid the arrival of light and the photocurrent generation are able to reduce Voc [8,9]: reductions in transmittance of the covering glass i.e., breakage, excess of ultraviolet illumination; encapsulant browning, delamination; corrosion or degradation of the anti-reflection coating; defects that avoid the generation of electron–hole pairs, like doping defects, impurities, dislocations, cracks, grain boundaries.

Ohmic shunts [11,24] imply the creation of parallel pathways of low resistance through the pn-junction or by the edges of the cells, connecting both sides of the junctions. Ohmic shunts follow the linear Ohm's law and are represented by the shunt resistance (Rsh) of the cell models.

Voc may also be reduced by processes that accelerate recombination, most of them associated to defects in the semiconductor structure like those of the large list just mentioned, since recombination and electron–hole pair generation are strongly linked. Non-ohmic shunts [11,24] follow non-linear exponential-type laws, and are associated to defects inside the depletion zone of the junction that cause an excess of recombination. An effect that increases with temperature and that is represented by the second diode in the two-diode model, considering an ideality factor greater than 2.

Shunts are induced by defects in the material structure [25], by the manufacturing process [24] and by environmental causes. Material-induced shunts are not predominant. They are due to crystallographic defects mainly in grain boundaries and bulk areas. Most of these defects are non-ohmic. Process-induced shunts are mostly ohmic, like cracks, poor isolation at the edges and corners of the cells, faults in the metallization process with diffusion of metals in the semiconductor, presence of contaminants like Al particles [11]. In this case, non-ohmic shunts are also found like those induced by scratches at the surface of the solar cells.

Concerning environmental factors [26], the ingress of moisture reduces the resistance of materials and is able to increase leakage currents by reducing shunt resistance. Temperature may affect the speed of recombination processes. Shading, snow covering or soiling, can create ohmic type shunts. When cells are forced to work at a current higher than its short-circuit current, they enter reverse bias, consume power, create hot spots that damage the cell and create shunts. This mechanism is also present in cells with potential-induced degradation (PID) [27], adding additional deterioration to the cells. Bypass diodes mitigate damage but do not avoid it.

I-V curve analysis [28,29], electroluminiscent and infrared termographies and isolation tests, are the main tools to study shunts. Shunts causes heating of the affected solar cells that can be detected by thermal cameras focused on the near infrared (5000–13,000 nm) [30–33]. On the other hand, electroluminescent techniques consist of the application of inverse voltages in the junction box that inject currents close to the short-circuit current, giving rise to the electroluminescence of the solar cells in a more distant infrared (850–1700 nm). The presence of shunts causes the failure of the electroluminescent emission of the cells, even the blackout of the cell in the image [34,35]. Procedures to distinguish between ohmic and non-ohmic shunts has been developed [36] with these technique. Both thermography or electroluminescence have been accepted as tests to confirm PIDs, and in the case of thermography, with tests in the laboratory or in the field [37,38]. The loss of control on the current paths when shunts develop, is a common cause of loss of insulation appearing leakage currents to the frame, especially with shunts created in the edges of the cells. Several simple methods to measure insulation resistance are presented in the literature [39], most of which are based on the standard IEC 61215:2005 10.3.

2.1. Potential-induced degradation

This section presents the effects of potential-induced degradation (PID) that are important to this paper because they are found in the plants. General reviews are available in the literature [40–44].

Potential-induced degradation (PID) is a widespread problem that causes lower performance of solar modules. There are 3 types of PID;

PIDp (polarization), PIDc (corrosion) and PIDs (shunting). In general, high string voltages cause very high voltage gradients between the semiconductors and the module frame, which can cause leakage currents that affect the recombination process at the pn junction [45,46] and the consequent loss of voltage and power that has been quantified around the range 27%–39% [47,48].

PIDp [49,50] is caused by a degradation of the pasivation layers when the cell is subjected to high positive voltages (in n-type cells) with respect to the frame. Positive charges from the EVA, crystal, etc., accumulate before the passivation layer and affect the electric field in the opposite region of the layer in the semiconductor, increasing recombination [42] and reducing Voc and short-circuit current (Isc). PIDc is due to corrosion caused by the presence of oxygen in the semiconductor and/or in the passivation layer during the fabrication process, forming silicon oxides that induce mechanical stresses in the semiconductor and in the passivation layer [51,52]. Voc and Isc are reduced because of the loss of electrical properties of passivation that promote recombination and if the corroded area grows significantly, the effective surface of the cell is reduced.

PIDs is the most common type of PID. Especially in the case of standard crystalline Si (cSi) modules such as those discussed in this article. This is mainly attributed to the reduction of the shunt resistance [53]. Pathways whereby small leakage currents to the ground are settled. In cSi p-type panels, currents flow from the frame, which is generally grounded, to the cover glass, encapsulant, antireflective coating, and finally the semiconductor. In fact, there are multiple leakage pathways that also involve the back-sheet and sides of the module. Leakage currents are very small and are produced by the migration of sodium Na^+ ions [54,55]. K^+ ions has been also reported to be involved [56]. Na^+ ions are initially contained in the materials of the panel such as soda-lime glasses or from manufacturing contaminations, and migrate toward the semiconductor material, where they accumulate and grow inside semiconductor defects such as dislocations or other existing faults in the crystalline structure. These Na^+ decorated defects cross the depletion area creating shunts. The potential barrier of the pn junction is lowered, resulting in a voltage drop in the panel and its delivered power [56]. This drop affects the open-circuit voltage (Voc) of the module [10,38,47,57], so that it can be used as an indicator of PIDs [58]. The migration of sodium ions through the materials does not occur homogeneously, but in specific areas, leading to localized shunts [41]. The absence of Na ions in the glass has been shown to reduce PIDs but not to eliminate it [59]. This is one of the strategies to avoid PIDs, along with creating barriers in the anti-reflective coating, or improving the isolation of the frame, but there are negative side effects or the cost effectiveness is compromised [60]. In the case of the cSi n-type, the effect is similar, with leakage currents in the opposite direction, from the semiconductor to ground, and migrating ions being negatively charged. This kind of PIDs is of ohmic type and is the main mechanism, but non-ohmic PIDs is also involved when defects do not cross the depletion area, promoting high recombination rates [41].

In cSi p-type modules, due to the direction of the currents (grounded frame to semiconductor), the effect is fostered when the panel is subject to negative voltages relative to ground and reduced when voltages are positive [58]. This is the reason why PIDs predominantly occurs in the parts of the string with negative voltage. In n-type panels, the opposite occurs.

Most modern converters are transformerless. They usually divide the total voltage into quasi-symmetric positive and negative branches, with approximately 0 V in between (floating voltage). With transformer-type converters, any pole can be grounded. The negative pole of the voltage can be grounded so that the entire string is subject to a positive voltage and PIDs can be reduced in cSi p-type plants [41].

The effect of moisture and temperature on PIDs has been studied [61,62] and is referred to as the main driver of PIDs. During the early morning hours, moisture and dew promote the effect by increasing the conductivity of the cover and frame. At this time PIDs can be quite homogeneously distributed in any part of the panel. When the sun rises and dries the panel, this effect occurs especially in the cells closest to the frame and in those with the most negative voltage (p-type). If moisture settles inside the panel, the effect remains in the long-term reducing the resistance of materials included silicon and droping Rsh. On the other hand, at a constant humidity level, PIDs increases with temperature [63]. In addition, there is usually a higher degradation in hot climate areas with large intraday differences in temperature. In summary, string voltage, humidity and temperature are main factors influencing the intensity of PIDs.

PIDs can sometimes be reversible. If reverse voltages are applied to the panel, the migration of ions in the opposite direction is achieved [64,65]. On restoring the standard operating conditions, the ions return to the semiconductor again through the pathways and the PIDs reappears. In addition, it has been shown that this second restoration of PIDs is faster as migration channels remain settled. It has also been reported that in-field anti-PID systems stop degradation but do not produce recovery to initial conditions [47]. On the other hand, PIDp is reversible and PIDc is not.

Both thermography or electroluminescence have been accepted as tests to confirm PIDs, and in the case of thermography, with tests in the laboratory or in the field [37,38]. I-V curves of a panel with PID also present a characteristic pattern [28], where there is a tendency to have measurements below the nominal voltage under standard conditions and a more progressive and less abrupt fall of the curve. Likewise, the flat part of the I-V curve tends to be slightly lower, offering less current than the healthy panel.

Regarding insulation tests on PID cases, the power loss of the modules has been reported to be proportional to the leakage current [66,67], so that PIDs reduces the isolation level of the panel.

Concerning the PID condition of the case-study plants, the authors have not found similar in-field cases of such severe level of degradation in the literature review. Authors observe an initial problem of PID that evolves negatively resulting in a stronger degradation that can go beyond PID, but mainly related with shunt creation. Most previous studies of PID in the last decade were laboratory studies reporting short-term effects induced by rapid degradation techniques. Currently, there is an increasing interest in-field conditions looking for the long-term effects, where the power loss of the modules and string are reported to be caused by voltage rather than current drops, stating that the Voc drop is a clear effect of PID [10,47,57]. Severe PID affection has been associated as a source of hot spots in the modules [27,48].

3. Materials and methods

A description of three case studies and the procedures that were performed is presented: description of the plants, measurements of monthly energy production, in-field determination of failure condition before repowering the plants, and subsequent laboratory tests to confirm it.

3.1. Description of the solar plants

Three photovoltaic plants are presented, plant no. 1, 2, and 3, respectively (Fig. 1, view of plants 1 and 2). They are grid-connected, but their main purpose is to supply power to three respective agricultural water pumping facilities of 75 kW each, watering very intensively in spring and summer. The plants are in the region of Andalucia (Spain), province of Córdoba (northern Andalucia). It is an inland province, with hot Continental-Mediterranean climate. In winter the mean temperatures in the years 2017–2019 were about 8–10 °C with mean maximum temperatures of 12–17 °C, and in summer, mean temperatures of 26–29 °C, mean maximum temperatures of 34–38 °C, reaching maxima of 42 °C. Springs are short, with rapid transitions from winter to summer weather. The levels of solar irradiance are among the highest in Spain and Europe, with a mean global and

Fig. 1. Aerial views of plant 1 (up) and plant 2, the last one with two maintenance operators on the roof.

Table 1
Features of the solar modules.

Max. power	Voc	Isc	Vmp	Imp	NOCT
175 W	42.6 V	5.52 A	35.5 V	4.93 A	48°C

Voc, Isc: open-circuit voltage, short-circuit current.
Vmp, Imp: voltage and current at maximum power at STC.
NOCT: Nominal Operating Cell Temperature.
Monocrystalline silicon p-type.
72 cells (12 × 6) of 125 × 125 mm each, in 3 substrings
Encapsulant: EVA 0.5 mm. Backsheet: TPT, Tedlar.
Size: 1580 × 808 × 46 mm (1556 × 784 without Al frame).
Warranty: 90% of power in 10 years, 80% in 20 years.

direct daily irradiance between 1985–2005 in July of 8.12 and 6.23 kWh m^{-2} day^{-1}, in December of 2.23 and 1.48 kWh m^{-2} day^{-1}, with a mean value of 5.12 and 3.59 kWh m^{-2} day^{-1} over a 20-year period [68]. The level of annual precipitation in the area is low 589 mm, as well as its average humidity, although it increases in the areas close to the Guadalquivir River, one of the main rivers of Spain, and the irrigation zones around it.

Plant 1 is in the town of Montoro, whereas plants 2 and 3 in Cardeña, both towns separated 35 km away. Montoro has the highest registered temperature in Spain ever, so it is one of the hottest areas in the Spanish summer. Plant 1 is close to the Guadalquivir River. The three plants were designed and built simultaneously by the same installer using the same solar panel and inverter model. All panels were purchased at the same time in a single order to the same manufacturer in 2008, as the inverters were to the correspondent supplier. The plants are installed on the roofs of different new agro-industrial facilities designed to optimize the solar installations. The commissioning of the three plants was in summer 2009. The panels are made of p-type monocrystalline silicon. Tables 1–3 show the features of the modules, inverters, and plant configuration. The manufacturer's specifications guaranteed a maximum power loss of 10% after 10 years and 20% after 25 years.

The inverters are transformer-type, showing floating voltage. Therefore, half of the string is subject to negative voltage up to about −300 V, a condition that is able to promote PID.

3.2. Performance of the plants

O&M (operation and maintenance) was performed by the installer, applying similar O&M plans in the three plants. Monthly measurements

Table 2
Features of the inverters.

Power (kWp)	Vmax (V,dc)	Mppts (pcs.)	Idc (A)	Iac (A)	Vac (V)	AC Power (kW)
110	900	2	230	145	3 × 400	100

Inverter with transformer, one per plant.
Idc: maximum DC intensity. Iac: AC current output at Idc input.

Table 3
Features of the plants.

Plant	Power (kW)	Strings	Panels	Voc (V)	Vmp (V)	Strings	Mppts
1	114.8	41	656			20	21
2	106.4	38	608	681.6	568	19	19
3	106.4	38	608			19	19

16 panels/string. All panels 19° tilted.

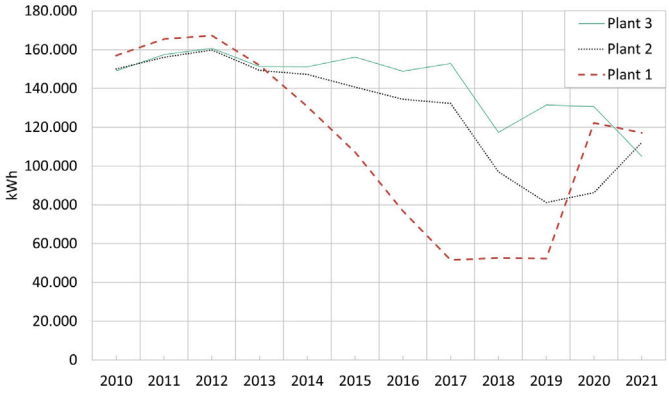

Fig. 2. Evolution of the annual production of the three plants.

of energy production have been monitored for 12 years, from 2010 to 2021. Fig. 2 shows the evolution of the total annual production of the plants. It is observed that plant 1 starts an intense degradation four years after commissioning that lasts for another four years, stabilizing the production and generating in 2019 only 32.48% of the average annual energy in the first four years of operation. The recovery of the last years is due to the repowering project. Plant 2 begins its degradation in the fifth year, with a minimum production of 52.78% in 2019 related to the average annual production of the first four years. A partial repowering improved production in the last year. However, plant 3 maintains a better production level for 7 years, although slightly decreasing, showing an annual production of 75.88% in 2018 compared with the first four-year mean, and reaching 67.94% in 2021. These respective production drops of 67.58%, 47.22% and 32.06% in the tenth year are significantly higher related to a 10% reduction in power given by the manufacturer's warranty.

Fig. 3 shows the monthly production of each plant. The progressive degradation is observed. Additionally, it should be expected that May, June and July will be the months with higher production, a pattern that is lost while degradation progresses. The production of plant 1 (the most degraded plant) from 2015 onwards was higher in winter than in spring and summer, giving the lowest scores in summer 2016, 2017 and 2019.

All data are available in a spreadsheet in open access mode [69].

3.3. Methods to assess degradation and description of the repowering project

3.3.1. In-field measurements

In 2019, a repowering project was launched that included an assessment of the degradation of the three plants, and the replacement of the most degraded panels: 246 modules out of 656 (37.57%) in plant 1

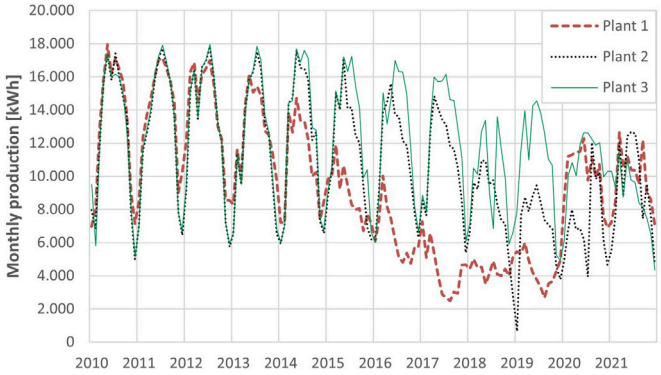

Fig. 3. Monthly production of the three plants.

Table 4
Substitution plan of plants 1 & 2.

Year		Plant 1	Plant 2
2019	Modules	224	
	Strings	14	
2020	Modules	32	138 new+6 old
	Strings	2	8+1 hybrid[a]
2021	Modules		**48**
	Strings		**3**

[a] Hybrid: string mixing new and old modules.

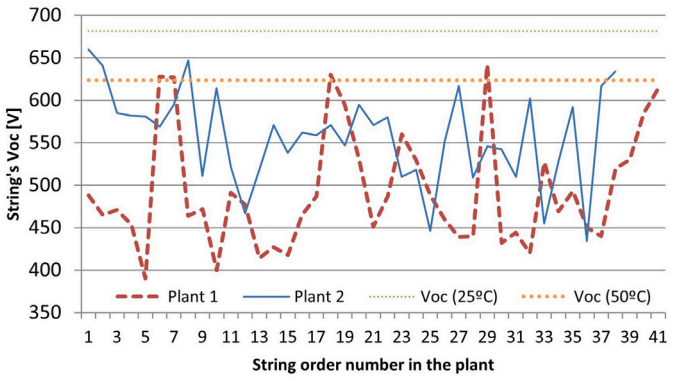

Fig. 4. Measured open-circuit voltages in the strings of Plants 1 & 2. Horizontal dotted lines: thin, string Voc in standard conditions; thick, increasing to 50 °C (β_{Voc} = −0.34%/°C).

and 186/608 (30.59%) in plant 2. The repowering partially recovered production in 2020 to 73.04% of the mean of the first four years in plant 1 and 72.88% in plant 2 by 2021.

The project was divided into three successive phases, one for each plant, starting from the most affected one (plant 1) and finishing with the least one (plant 3). The project is expected to be completed by 2025. The new panels were mounted to form full new strings, reorganizing the location of the remaining old panels. At the time of writing this paper, the repowering of plants 1 and 2 was completed under the scheme indicated in Table 4. The main replacement of panels in plant 1 was carried out in August 2019 and completed in August 2020 and for plant 2 in July 2020 and completed in May 2021. In this last installation in May 2021, a purchase of 48 panels was ordered in October 2020, based on the model shown in this paper.

In plants 1 and 2, the total Voc of the strings was measured (see Fig. 4). Variations of about 200 V can be observed among the highest and lowest voltages of the strings in each plant. Plant 1, average 493.04 (±67.56) V, plant 2, 557.87 (±54.34) V, averages representing 72.3% and 81.8% of the nominal Voc (681.6 V).

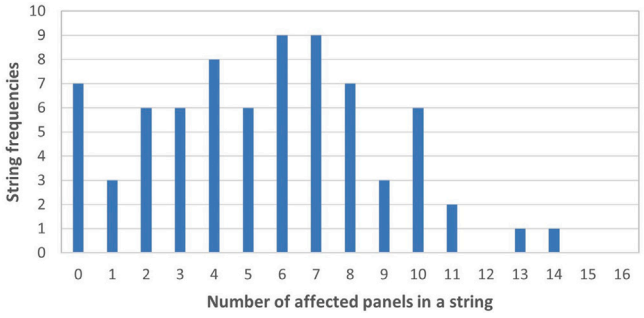

Fig. 5. Frequencies of the number of affected panels by string in the available data set, counting as affected panels, those in the families of 26 V and 12 V.

Table 5
Features of the new solar modules.

	Pmax (W)	Voc (V)	Isc (A)	Vmp (V)	Imp (A)	NOCT (°C)
Old	175	42.6	5.52	35.50	4.93	48
Plant 1	195	45	5.45	38.30	5.09	47
Plant 2	200	45.2	5.53	38.71	5.17	47

Monocrystalline silicon p-type.

The Voc of every panel in each string of plant 1 was checked, just before changing the panel if degraded. Two families of voltages around 26 V or less (248 out of 656 panels, 37.8%) and around 40 V (408, 62.2%) were found. The exact voltage of every panel was not recorded, but the number of panels in every voltage family by string. After the repowering of plant 1, a new group of voltages centered in 12 V was noticed, but they were reported as "<26 V".

In the second plant, and after these results, the three voltage families were recorded, showing panels with 12 V (61 out of 528 measured, 11.5%), 26 V (95, 18%) and 40 V (372, 70.45%). The degraded panels totaled 156 (29.5%), meaning degraded those with 26 V or less, assuming then a very high level of degradation to be considered as "degraded". In fact, after the repowering of plant 1, the degradation of the 40 V family (62.2% of the modules) remains because the annual production loss in 2021 related to the initial four-year average was still about 25%. This means that production loss is also present in the panels of 40 V family. It must be noted that a panel in the 26 V family is related to one inactive substring in the module with its bypass diode activated, and two substrings for 12 V family.

Fig. 5 shows the frequency distribution of the number of failed modules by string considering all strings of plants 1 and 2, with a mean of 5.46 degraded modules by string.

All new modules for repowering are from a different manufacturer than the initial one. Both plants install the same type of module but with slightly different features in plant 1 and 2, as shown in Table 5.

3.3.2. Laboratory tests

Laboratory tests were performed on three substituted panels. It consisted of a visual inspection, an outdoor infrared thermography test with the panels connected to a load, the recording of the I-V curves and an isolation test. Each of the three panels belonged to a different group of Voc families found, 40 V, 26 V and 12 V. In the case of the 26 V family, a second panel was included.

The thermography test was performed using a FLIR camera, model E6 1.2L, with a resolution of 160 × 120 pixels and a spectral range 7.5–13 μm. The panels were located outdoors at the ground level under full operating conditions. Thermal images were taken after more than one hour of operation. Images were treated to ease their integration into the paper layout (moving labels, the temperature scale and cropping). The images of the panel surfaces presented later are fully original.

I-V curves were measured with two standard lab multimeters using a variable resistor as a charge.

Finally, an isolation test was performed on the panels using the method described in [39]: the panel was covered in darkness. Both terminals are shorted and connected to the negative pole of a DC source. Positive pole to the ground. The frame to a 200,000 Ω resistor and finally to the ground. The voltage in the resistance is measured, and leakage currents are calculated using Ohm's law and the full shunt resistance. Source voltages: 1000, 500, and 250 V.

4. Models to estimate the number of degraded panels

Data collected from plants 1 and 2 consisted of pairs (Voc, N_{fail}), string open-circuit voltage, and the number of degraded panels in the string (with voltage around 26 V or less), counting 74 samples (strings) in both plants.

Linear regression was initially selected to model this relationship so that the number of degraded panels of a string could be estimated from its open-circuit voltage. Two main reasons support this decision,

- The string architecture determines an additive structure of the modules' voltage to form the string voltage, suggesting a linear component in the behavior.
- The ease of practical implementation.

As a drawback, the behavior at the panel level in terms of voltage drops in steps around three voltage families, as the substrings fail. This aspect is expected to add dispersion rather than breaking linearity, prevailing the string additive structure.

Once a linear regression method is implemented, a quadratic regression will be added without much effort. Both regressions will be applied with and without outliers, totaling four methods. Outliers will be considered by removing the furthest samples from the regression lines in the models adjusted with full data, and will be limited to a short number of samples. In any case, the aim of this work is not to look for the most efficient model for the estimation, it is the practical aspect of supplying simplicity and ease of implementation.

The methods are initially fitted with data from plant 1, giving regressions P1L (linear), P1Q(quadratic) and without outliers P1LO, P1QO. Equivalently, fitting with data from both plants, the models are P12L, P12Q, P12LO and P12QO.

5. Results and discussion

In this section, the results of the laboratory tests, their interpretation, and regression models are presented.

5.1. Lab testing

The three panels were selected from each family of voltages: 40 V, 26 V and 12 V. An important number of panels from 26 V and 12 V families gave a Voc measure of about 40 V in the initial exposition to the sun, failing in few minutes. Other panels directly failed from the beginning. No panel presented 0 V in the Voc measurement.

Selecting three panels, one from each family, Table 6 shows measurements made in July 2022 on their Voc just taken out from dark storage, after 5 min of sun exposure and 15 min (irradiance 915 W/m^2). The panels were previously tested in July 2021 after their decommissioning and remained stored throughout the year. The panel named 26 V-A of the 26 V family was assigned to that family in July 2021 without doubt. On the first day of testing in July 2022 (a year later), the panel showed an initially recovered Voc. After 15 min of sun exposure, the panel gave a measure of 26 V. After two hours under the sun, it recovered to full voltage. Three days later, a new test was performed (Table 7, irradiance 932 W/m^2). The panel showed a Voc of 40.3 V in the initial moments of insolation, rapidly failing for the rest of the time to a maintained level of around 26 V. Given this varied behavior, another panel of the 26 V family (26 V-B) was also considered. This effect is also observed in field, where these types of modules initially show a Voc around 40 V and they start failing to 26 V when irradiation increases. It seems that from a certain temperature, the failure of the substrings appears. This in field behavior of the failing modules is predominant in the hottest months of the year but not in the coldest, when they maintain a good voltage of around 40 V, something that seems to be confirmed by the monthly production of the plants of the last years (Fig. 3). Although the frequency of this effect has not been measured in field, it is so common as to make the decision to measure the open circuit voltages in the hottest months to detect the failing modules.

Fig. 6 shows the I-V curve of the panel in the 40 V family in dashed style and the curve given by the manufacturer in dotted style. The manufacturer only supplied a curve for a similar panel of 165 Wp and this curve was recalculated for the 180 Wp panel to obtain the dotted curve. In continuous line, panel 26 V-A tested with its recovered voltage on the first day of testing in July 2022.

Fig. 7 depicts the I-V curves of the 26 V and 12 V families on the second day of testing. Dotted curves are the manufacturer's curve with the voltage multiplied by 2/3 (gray) and 1/3 (black), representing

Table 6
First day of testing July 2022. Open-Circuit measurements before permanent conditions.

Before sun exposure, in the shade, Irradiation 40 W/m^2					
Family	Voc (V)				Panel
	Panel	Substr.1	Substr.2	Substr.3	temp.
40 V	36.6	12.1	12.2	12.1	29.2 °C
26 V-A	37.3	12.4	12.4	12.4	28.3 °C
12 V	11.5	1.9	1.1	12	27.7 °C

Family	After 5 min., 915 W/m^2		Ater 15 min., 915 W/m^2	
	Voc (V)	Temp. (°C)	Voc (V)	Temp (°C)
40 V	39.7	52.2	39.4	56.1
26 V-A	40.3	50.8	26.0	54.7
12 V	11.3	45.3	12.6	53.7

Environmental temperature: 27 °C.

Table 7
Second day of testing July 2022. Open-circuit voltage (V).

Family	Initially	After 2 h sun exposure, 932 W/m^2			
	Panel	Panel	Substr.1	Substr.2	Substr.3
26 V-A	40.3	25.4	0	12.7	12.7
26 V-B	26.4	25.8	12.8	0	13.0
12 V	16.4	17.5	5.5	0	12.5

Environmental temperature: 29 °C.
Note: substring 1 is always the left one in the thermographic images.

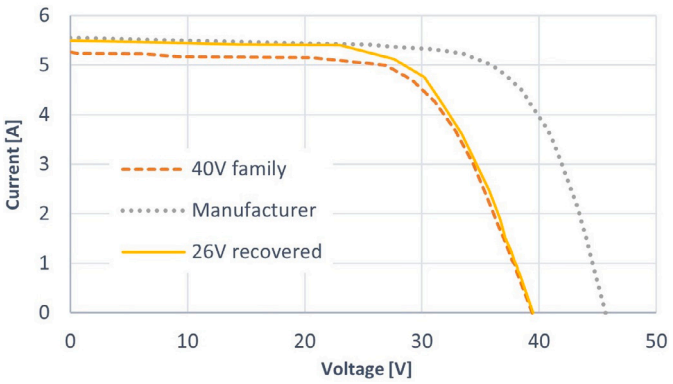

Fig. 6. Curve IV. Two panels with a voltage around 40 V. The continuous line is a 26 V family panel (26 V-A) that recovered its voltage after one-year storage.

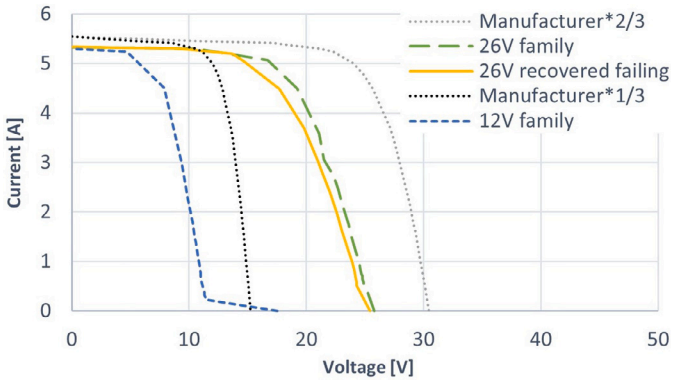

Fig. 7. Curve IV of panels of 26 V and 12 V families. Dotted lines for reference. Continuous line: panel 26 V-A, recovered after one-year storage failing again 3 days later. Failure remained the following days. Long-dashed: panel 26 V-B.

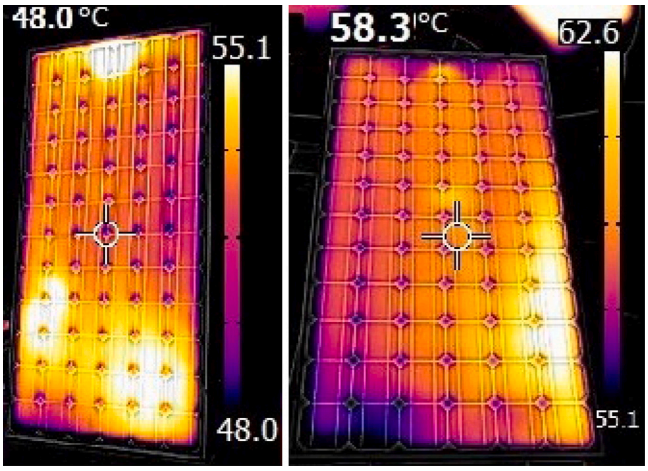

Fig. 8. Thermography. Left: panel of the 40 V family (24/03/2021). Right: panel of 12 V family (11/07/2022).

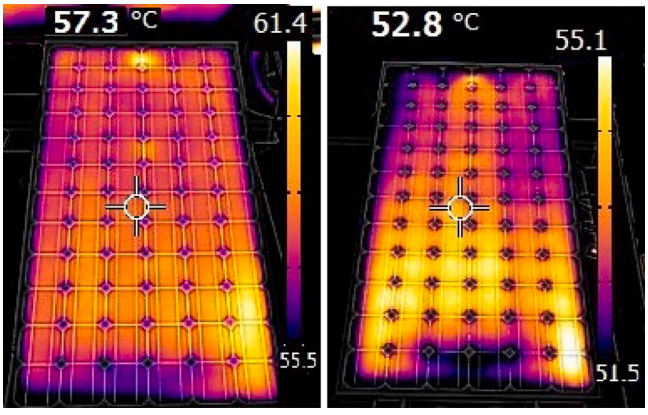

Fig. 9. Thermography (11/07/2022). Left: panel 26 V-A. Right: panel 26 V-B.

the original curves for two and one substrings, respectively, just for comparison. In continuous line, panel 26 V-A failing again and panel 26 V-B in long-dashed style. In short-dashed line, panel of 12 V, where it is observed an Voc of 17.5 V (one substring in short-circuit) and 11.4 V as soon as a charge is connected, failing a second substring. The measurements of Voc on this second day are in Table 7.

Table 8
Isolation test.

Source (V)	Family Panel	Resistance Volt.(mV)	Leakage Curr.(mA)	Isolation (MΩ)
1000	40 V	3.62	18.1	55,249
	26 VB	7.30	36.5	27,397
	26 VA	12.15	60.75	16,641
	12 V	15.89	79.45	12,587
500	40 V	1.20	6.0	83,333
	26 VB	2.32	11.6	43,103
	26 VA	4.48	22.4	22,321
	12 V	6.12	30.6	16,340
250	40 V	0.56	2.8	89,286
	26 VB	0.80	4.0	62,500
	26 VA	1.75	8.75	28,571
	12 V	2.40	12.0	20,833

Environmental temperature: 13.1°C; Humidity: 50.4%.
Surface of the panel without frame: 1.215 m^2.

Thermography images were taken with the panels under operation. Fig. 8 presents thermographic images of the panel of the 40 V family (left) and 12 V family (right). Fig. 9 shows 26 V-A (left) and 26 V-B (left). A panel in good condition should show a continuous temperature distribution. PID is usually expressed at higher temperatures of the cells more commonly at the bottom half of the panel (not only) and many times close to the frame (not always). The junction box of the modules can be observed at the top center of the images as a hotter point. Junction box apart, all the hot areas of the panels are in the bottom half of the modules. The 40 V panel shows two areas of higher temperatures, quite close to the frame. The 12 V panel presents a hot area in substring 3, the only one working, at cells close to the frame. The module 26 V-A (left) has the hottest area on the lower right side, again close to the frame, as well as panel 26 V-B in the same corner. This panel also presents high temperatures in the left and central areas of the bottom half. With due caution, these remarked effects are compatible with PID. The temperature of the modules has also been related to the level of PID affection. Looking at the temperature scales of the images, panel 12 V, with higher damage, is clearly the hottest, followed by the 26 V-A. The 40 V and 26 V-B modules show similar scales and temperatures. The temperature indicated in the image is that of the central cross-pointer, which can be used for comparison. The central substring with the active bypass diode in the 26 V-B panel is clearly visible. Although not so clear at 12 V, the color structure of the central substring is compatible with that of an active bypass diode. It is not so clear in the case of 26 V-A (substring in the left).

The results of the isolation test (Table 8), shows a reduction of the isolation level as the panel fault level increases. Voc and isolation resistance show an almost linear relation in the panels 40 V, 26 V-B and 12 V in each of the three voltages applied by the source. This linearity is not the case when exchanging 26 V-B by 26 V-A, but the reduction of Voc with isolation resistance clearly remains in all the voltages of the source. This result is also compatible with the degree of PID affection.

Panel 26 V-A was thoroughly studied, given its strange behavior. The total Voc measure was 25.6 V, and the readings of substrings 1, 2 and 3 were −0.6 V, 13.0 V and 13.2 V, indicating the activation of the first bypass diode. The voltages of the 24 cells of substring 1 were measured, after a previous local removal of the back-sheet to access the busbars at the interconnections of the cells. This operation is delicate; therefore, the result could lead to certain errors in the readings. The nominal Voc of the module, substring and cell are 42.6 V, 14.2 V and 0.59 V. The voltage readings in the cells of the substring were: 0.56 V in 9 cells, 0.55 V in other 9 cells, 3 cells 0.54 V, 2 cells 0.53 V, totaling 12,67 V (mean 0.5508 V) and a cell bias reversed with a reading of −12.86 V. The location of this cell is on the second bottom row, second column from the left, a cell that does not appear hot in the thermography. The extraction of the first bypass diode gave a reverse

Table 9
Regression models adjusted with data from plant P1, linear (L) and quadratic (Q), considering full data or removing four outliers (O) with initial residuals higher than 3.5 solar modules.

Parameter	P1L	P1Q	P1LO	P1QO
Pearson corr.	−0.806517		−0.885054	
P-value	$1.95 \cdot 10^{-10}$		$3.58 \cdot 10^{-13}$	
Intercept	26.8058	**19.0526**	27.5884	21.6832
Linear coef.	−0.0421014	**−0.0117032**	−0.04352	−0.020541
Quadr. coef.	—	**−2.92116** $\cdot 10^{-5}$	—	$-2.19184 \cdot 10^{-5}$
RMSE	2.0849	2.0805	1.5525	1.5495
R^2	0.6505	0.6519	0.7833	0.7842
Adjusted R^2	0.6415	0.6430	0.7771	0.7780
F - statistic	72.57	73.04	126.53	127.15
P (*F*-statistic)	$1.95 \cdot 10^{-10}$	$1.79 \cdot 10^{-10}$	$3.58 \cdot 10^{-13}$	$3.34 \cdot 10^{-13}$

In bold letters, model used in practice (quadratic, outliers included).

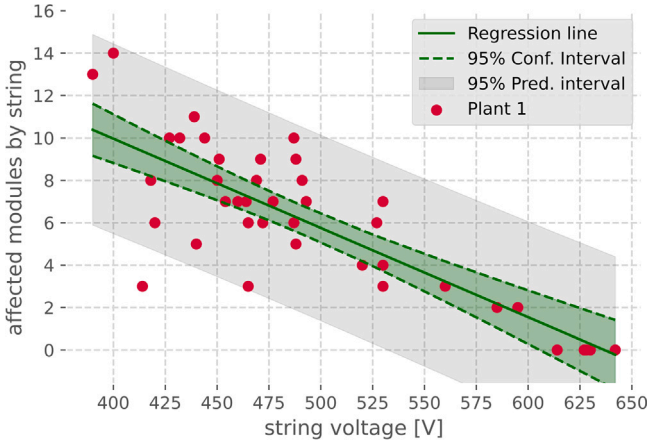

Fig. 10. Regression model P1L: linear case. Data: Plant P1.

bias in the same cell of −38.9 V, reversed −26.4 V in substring 1, annulling the total voltage of the module. The three bypass diodes were checked in the lab, showing correct working; conduction from about +0.5 V and no current in reverse bias tested in the range [−30,0] V, when under normal operating conditions they withstand −10 V to −15 V.

5.2. Estimation of the number of degraded panels measuring the string voltage

The collection of data was done in-field, being the string voltage the independent variable and the number of failed modules per string as the dependent variable. After the repowering of plant 1, the first set of real data was available to adjust the first version of the model.

Table 9 shows the fit of the least squared regressions with data from plant 1, both linear (model P1L) and quadratic (P1Q). Two additional versions of them (models P1LO and P1QO) are presented by removing outliers, four samples out of 41 strings with absolute values of residuals greater than 3.5 modules. The four samples resulted in two extreme strings on both sides of the regression lines.

The variables presented a Pearson's correlation coefficient of −0.807 and a *p*-value $1.95 \cdot 10^{-13}$, showing high dependence and a significant statistical relation, respectively. Removing outliers, the correlation improved significantly to −0.885 (*p*-value $3.58 \cdot 10^{-13}$).

The linear and quadratic regressions (P1L and P1Q) are shown in Table 9 and Figs. 10 and 11. A quite acceptable adjustment is achieved since the coefficients of determination (R^2) are respectively 0.6505–0.6519, showing that about 65% of the variability of the number of wrong modules per string is explained by the variability of the open-circuit voltage of the string. These R^2 coefficients and their adjusted versions (0.6415–0.6430) are quite close, indicating the high

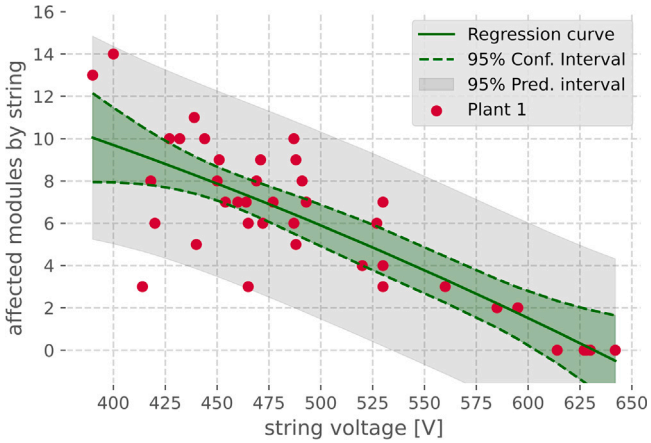

Fig. 11. Regression model P1Q: quadratic case. Data: Plant P1.

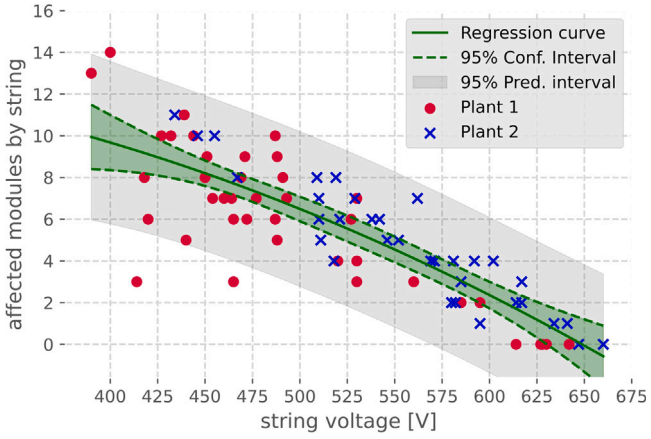

Fig. 12. Regression model P12Q: quadratic case. Data: Plants P1& P2.

Table 10
Regression models adjusted with data from plants P1& P2, linear (L) and quadratic (Q), considering all data or removing four outliers (O) with initial residuals higher than 3.5 solar modules.

Parameter	P12L	P12Q	P12LO	P12QO
Pearson corr.	−0.835124		−0.904957	
P-value	$2.27 \cdot 10^{-20}$		$1.46 \cdot 10^{-26}$	
Intercept	25.893070	12.917076	28.06458	20.369255
Linear coef.	−0.0392037	0.0108792	−0.042911	−0.0134874
Quadr. coef.	—	$-4.74498 \cdot 10^{-5}$	—	$-2.76571 \cdot 10^{-5}$
RMSE	1.8270	1.8132	1.3847	1.3791
R^2	0.6974	0.7020	0.8189	0.8204
Adjusted R^2	0.6932	0.6978	0.8162	0.8177
F - statistic	166	169.6	303.05	306.10
P (*F*-statistic)	$2.28 \cdot 10^{-20}$	$1.32 \cdot 10^{-20}$	$1.46 \cdot 10^{-26}$	$1.11 \cdot 10^{-26}$

importance of the regression parameters in the dependent variable. There is a slight difference between the linear and quadratic models. Important improvements are again obtained by removing the outliers (R^2 78.3%, Adj. R^2 77.7%), indicating a higher impact between variables. There persists a weak difference between the linear and quadratic versions.

Fig. 12 and Table 10 show the regressions fitted with all data from plants 1 and 2 (models P12-). The distribution of the samples of the two plants shows the lower deterioration of plant 2, contributing the new data to improve the model fit in the right part of the graphic with higher Voc. The higher dispersion of the data from the most deteriorated strings of plant 1 seems to suggest that the higher the deterioration of the string voltage, the higher the dispersion of the data.

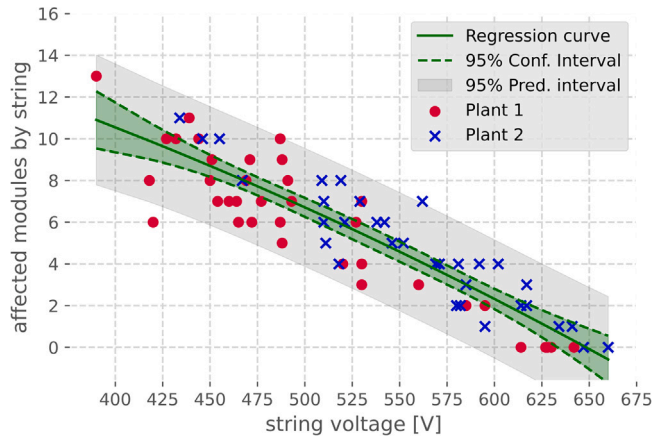

Fig. 13. Regression model P12QO: quadratic. Data: Plants P1& P2 removing four outliers.

These models improve the metrics, first with the data, being Pearson's correlations of 0.835–0.905, considerably higher, and second with the models, being R^2 0.6974–0.7020 (linear–quadratic) and without 4 outliers R^2 0.8189–0.8204. In this case, there are also 4 outliers, all from plant 1, but now 3 of them are under the regression line, one above. Fig. 13 shows the quadratic model removing outliers.

Models adjusted with data from plant 1 (models P1-) can be applied to estimate the number of failing modules in plant 2, entering the string voltages. The results are root mean square errors (RMSE) of 1.726 modules (P1L) and 1.706 (P1Q), both lower than the RMSE of the training data (around 2.08 in both), demonstrating the lower scattering of the data from plant 2 given its lower level of deterioration. For models without outliers, the RMSEs of predictions are 1.719 (P1LO) and 1.704 (P1QO), which are higher than those of the training data (around 1.55 in both models). All these RMSEs do not consider the estimation to be an integer number, although the results do not differ significantly (1.723 for P1L and 1.732 for P1Q).

In real practice, the model P1Q was used to place a purchase order of modules in winter 2020–21 for the second repowering intervention on plant 2 in July 2021, marked in bold letters in Table 4. The plant was subject to a previous partial repowering replacing 138 modules in summer 2020. These panels were arranged to form new full strings. After this intervention, 18 strings were left untouched, and their Voc were collected (see Table 11) to initiate the second repowering action of this plant. Therefore, data collection was done in summer 2020 to ensure that PID is expressed intensively. The order was placed without going up to the roof to check the number of wrong modules. This check was subsequently carried out in July 2021, when they were installed. The results are shown in Table 11. In this specific case, the total error in the estimation of failed modules results null, because under- and over-estimations are compensated, being the absolute error 10 out of 52 failed modules and a total of 288 modules in these strings. Ten strings out of 18 showed no discrepancy between reality and the model. Differences of two panels were found in two strings, where the model overestimated the failed panels, and variations of one panel in six strings, with five strings underestimated and one overestimated.

The presented model has also been used to initiate the repowering of plant 3. A purchase order of 96 panels has been placed based on the model results, just measuring the string Voc voltages in the control cabinet.

6. Discussion

6.1. Assessment of module degradation

The review of evidences to remark are the following,

Table 11
Repowering of plant 2: second action (July 2021). Blind purchase based on the results of the model P1Q.

String	Measured Voc (V)	Damaged panels		Model error (e)
		Model	Real	
1	629	0	0	0
2	612	1	1	0
3	547	4	3	1
7	571	3	1	2
8	622	0	0	0
10	598	2	2	0
17	543	4	4	0
18	553	4	5	−1
19	516	5	6	−1
20	556	4	4	0
21	549	4	5	−1
22	587	2	2	0
24	505	6	4	2
27	566	3	3	0
29	545	4	5	−1
32	569	3	4	−1
37	600	2	2	0
38	615	1	1	0
Total		52	52	0 ($\sum \lvert e_i \rvert$=10)

- Measurements in-field and IV curves in the laboratory show loss of voltage rather than current losses [47].
- Decreasing insulation resistance as the level of failure in the modules grows [67] in laboratory observations.
- Thermography: higher the temperature of the modules, the higher PID evidences are [37]. Presence of hot areas in the bottom half and tendency to be close to the frame.
- The presence of high negative voltage bias in one half of each string (up to −300 V) with p-type modules.
- Visual inspection revealed no obvious defects in most modules. A positive visual test would assign degradation to other cause.
- Gradual loss of annual energy production.
- Local conditions and weather prone to develop PID: very high temperatures in summer and late spring. Morning moisture, by proximity to the Guadalquivir River and its irrigation zones. Higher degradation in plant 1 that is considerably subject to higher temperatures and moisture levels. Similar behavior to other photovoltaic plants in this warm area that were affected by PID, being the most common problem.
- Seasonality of the produced energy, progressively decaying year on year, especially in the warmest months. Production in spring–summer ends falling below production in winter in the case of plant 1.
- The remaining 25% of energy loss after repowering panels of the 26 V and 12 V families.

Given these points, the possibility that plant degradation is primarily PID is remarkable. The proportional drop in insulation resistance with the intensity of the damage, together with the negative visual inspection, suggest a shunt type PID, which tends to be the most common. The panels of the 40 V family show a progressive drop in Voc, in which other causes, such as light-induced degradation, will initially appear, but continue to worsen. According to maintenance reports, when it reaches around 36 V, a bypass diode is triggered and the open-circuit voltage goes to around 26 V. The continuation of the process can cause the cancellation of another substring, forming the 12 V module family.

This process is highly dependent on the panel temperature, since in winter many panels recover the 40 V level when in summer they are at 26 V, an aspect that has also been described in laboratory tests. It has been shown that PID is highly dependent on panel temperature [41,63].

The failure mostly affects the panel voltage, a common issue in PID cases [56], although Isc is also affected. The non-uniformity in the

thermographic imaging pattern supports the evidence of PID, with hot areas in the lower half and some tendency to be close to the frame. Addinionally, most degraded modules show higher temperature. The drop in insulation resistance largely reinforces this evidence of PID. The presence of high negative voltages in part of the string with p-type panels is a necessary requirement that is met. The progressive drop in production over time, and the fact that after repowering (without panels of the 26 V and 12 V families), considerable degradation persists in the 40 V panels of about 25% in production drop, compatible with the power losses reported in PID cases. Finally, the environmental conditions of thermal variation, high temperatures and the dependence of the damage level on the humidity of the area are typical of the conditions that encourage the development of PID, with higher degradation in the plant that withstands worst conditions (plant 1). Electroluminiscence tests would have help to better determine the PID condition.

In short, PID is considered to initiate degradation and is reinforced by new failures or the deepening of failures already initiated by PID. It has been reported how PID can lead to other types of faults, such as the generation of hot spots, blackouts or microcracks [27,48]. With the help of voltage mismatching due to the parallel structure of strings that share voltage having non-uniform module behavior and the current mismatching among unbalanced serial cells in the string, damaged cells are forced to work under current levels that are higher than Isc, entering reverse bias, consuming energy and producing hot spots that generate new damage or enlarge the current one. Mosts times, this new damage causes a drop in shunt resistance and an increase in series resistance, as most types of degradation do. In fact, the drop in insulation resistance with degradation, is an indication that shunts grow.

When a cell enters reverse bias, bypass diodes trigger and avoid the evolution of damage to destruction, but the fact is that when the bypass diode acts damage is already done. Therefore, there is room for the failure to evolve before the bypass diode acts. A substring with an active bypass diode contributes neither to the addition of voltage to the string nor to the power delivery. Modules lose one third of the power and the voltage. New mismatches are promoted, new cells that are developing PID are under stress and new substrings become canceled.

6.2. Assessment of degradation at plant level

An aspect to remark in this work is that the threshold to define a failing module in the regression models refers to a very strong level of malfunction. The failure is not just the presence of PID, it is a second level of degradation where a substring is annulled by the activation of its bypass diode, so that the voltage of the module reduces by about one third, or two in cases of two substrings annulled. Therefore, this study is not proposing a method to detect the number of modules in the string with PID from the string's open circuit measurement, but the number of modules with a failing substring or more.

After repowering the improvement in production is known. Considering that in that moment all panels of families 12 V and 26 V has been removed, the percentage of production loss given by initial PID (family 40 V) and by higher damage can be roughly estimated. A standard annual loss of 0.8% in production will be assumed to account for the expected production drop without extra degradation, so that the expected production in the tenth year will be 148,011 kWh and 143,077 kWh for plants 1 and 2. Additionally, a correction for the higher power of the new panels will be applied, so that corrected increases are 62,878 and 52,392 kWh. This increase is given by 37.80% and 29.55% of the modules changed in both plants. This implies that the total production loss is given about 16% by the remaining panels of the family 40 V and 41% for failing modules in plant 1, and 21%–19% in plant 2. If all panels would be degraded in the level of family 40 V level, the loss of power would be about 23%–25% in each plant related to the average production of the four first years. This numbers are very compatible with reported cases of PID in literature [47].

With this complex pattern of failure, it has been observed that the production in plant 1 has become lower in the months of late spring–summer than in winter. This effect is not so extreme in plant 2, but is observed by the flattening of the interannual monthly production curves. The drop of the maximum monthly production has been clearly faster than the minimum monthly production during the years. This was the reason to test the failing modules is summer. This effect is due to the temperature dependence of the reverse bias entry of the cells and consequently the activation of the bypass diodes.

Since the definition of failure is bypass diode activation, the proposed estimation method would be useful in any type of failure leading to bypass activation, most of which end up in hotspot creation.

The sensitivity of the method with another less extreme definition of failure is a pending subject of study. It would be interesting to deep into an earlier detection capacity in the range of modules with Voc between 26 V and 42.6 V (family of 40 V).

The extension of the method to be applied in full production by measuring Vmp instead of Voc requires further development. The method has been designed to evaluate the string alone, in open-circuit, when it is normal to have several strings in parallel in the PV array. In such a case, one could think of a procedure with successive individual evaluations of each string while leaving the others in open-circuit, where the number of failing modules in the string under test could be estimated. Adding string power and current measurements could provide more monitoring capability. Such an implementation would imply the ability to put the strings in open-circuit by software individually, although it would not be necessary to put a voltmeter, wattmeter and ammeter on each string, it would be sufficient to use the general equipment of the PV array for each string when it is tested alone. It would be a complementary method to the current techniques for detecting PV array faults, like line-to-ground, line-to-line, bridging faults or module faults, etc., adding an estimation of the number of modules affected by the fault. The division of the expected string's Vmp by its current value, has already been used in estimations, but when it comes to situations in the field, the complexity increases and statistical estimations like the proposed method are valuable.

7. Conclusions

The main contribution of this work is twofold: (a) the development of a quick method to evaluate the number of affected panels, with practical application, and (b) the presentation of a highly degraded case describing the very long-term consequences of PID, given the limited literature found about these cases. Data are presented for three plants with very severe degradation. Apart from the typical variability of problems in a plant, the evidence and evolution of the behavior make PID and its long-term consequences to be the main driver of failure. PID may be induced in solar power plants in southern territories, near irrigable areas of flowing rivers, because of high summer temperatures and humidity. The severe degradation reaches the point where the substrings of the modules begin to fail and are annulled by the activation of the bypass diode, extending this problem to 37.8% of the modules in plant 1 and 29.5% in plant 2. This does not imply that the rest of the modules are in optimal conditions, when in fact recurrent reductions of around 5-3 V of the Voc with respect to the nominal value are observed. Likewise, the model can be used to rule out other types of failures in solar pumping systems, which in principle could be related to variable speed drive or line breaks, since the proposed model is easy to verify. But the main contribution is that it is born out of a real practical need; a quick estimation of the panels that are in a condition of failure, with no need to go up to the roof of the plant, avoiding long measurements of voltages module by module at times of danger of thermal shock for maintenance workers. In this way, the readings of the Voc of the strings in the protection cabinet facilitate the estimation of the number of panels in the described failure conditions. The method does not locate the failing modules in the string and it is starting to be used by the authors for the repowering actions of the plants.

CRediT authorship contribution statement

José Antonio Moreno: Writing – review & editing, Supervision, Resources, Project administration, Investigation, Formal analysis, Data curation, Conceptualization. **Rafael Muñoz:** Writing – original draft, Visualization, Validation, Resources, Methodology, Investigation, Formal analysis, Data curation.

Declaration of competing interest

The authors declare that they have no known competing financial interests or personal relationships that could have appeared to influence the work reported in this paper.

Acknowledgments

The authors would like to thank Mr. Evaristo Molero Mesa, technician head of the Electric Engineering Lab of the University of Granada (UGR), for his ideas and support during the last part of the experimental work and Dr. Enrique Alameda Hernández (Civil Engineering Dept., UGR) for his comments on the pre-submission version of the manuscript. This work has been supported by the authors and the University of Granada: the first author as a professional of O&M of the plants, and both authors as members of the UGR, using the means of the Electric Engineering Lab of the UGR.

Appendix A. Supplementary data

Supplementary material related to this article can be found online at https://doi.org/10.1016/j.solener.2025.113542.

Data availability

Data are published in open access mode with a doi available [69].

References

[1] P. Malik, R. Chandel, S.S. Chandel, A power prediction model and its validation for a roof top photovoltaic power plant considering module degradation, Sol. Energy 224 (2021) 184–194, http://dx.doi.org/10.1016/j.solener.2021.06.015.

[2] X. Ma, P. Ye, F. Gao, K. Zhou, K. Shen, Y. Zhang, Power output prediction of individual photovoltaic modules under operating photovoltaic system conditions, in: Lecture Notes in Electrical Engineering, Springer Nature Singapore, 2023, pp. 1068–1090, http://dx.doi.org/10.1007/978-981-99-0408-2.

[3] F. Rodríguez, F. Martín, L. Fontán, A. Galarza, Ensemble of machine learning and spatiotemporal parameters to forecast very short-term solar irradiation to compute photovoltaic generators' output power, Energy 229 (2021) 120647, http://dx.doi.org/10.1016/j.energy.2021.120647.

[4] S. Daliento, A. Chouder, P. Guerriero, A.M. Pavan, A. Mellit, R. Moeini, P. Tricoli, Monitoring, diagnosis, and power forecasting for photovoltaic fields: A review, Int. J. Photoenergy 2017 (2017) 1–13, http://dx.doi.org/10.1155/2017/1356851.

[5] S.R. Madeti, S. Singh, A comprehensive study on different types of faults and detection techniques for solar photovoltaic system, Sol. Energy 158 (2017) 161–185, http://dx.doi.org/10.1016/j.solener.2017.08.069.

[6] M. Aghaei, A. Fairbrother, A. Gok, S. Ahmad, S. Kazim, K. Lobato, G. Oreski, A. Reinders, J. Schmitz, M. Theelen, P. Yilmaz, J. Kettle, Review of degradation and failure phenomena in photovoltaic modules, Renew. Sustain. Energy Rev. 159 (2022) 112160, http://dx.doi.org/10.1016/j.rser.2022.112160.

[7] M.M. Rahman, I. Khan, K. Alameh, Potential measurement techniques for photovoltaic module failure diagnosis: A review, Renew. Sustain. Energy Rev. 151 (2021) 111532, http://dx.doi.org/10.1016/j.rser.2021.111532.

[8] G.R. Venkatakrishnan, R. Rengaraj, S. Tamilselvi, J. Harshini, A. Sahoo, C.A. Saleel, M. Abbas, E. Cuce, C. Jazlyn, S. Shaik, P.M. Cuce, S. Riffat, Detection, location, and diagnosis of different faults in large solar PV system—a review, Int. J. Low- Carbon Technol. 18 (2023) 659–674, http://dx.doi.org/10.1093/ijlct/ctad018.

[9] H. Al Mahdi, P.G. Leahy, M. Alghoul, A.P. Morrison, A review of photovoltaic module failure and degradation mechanisms: Causes and detection techniques, Solar 4 (1) (2024) 43–82, http://dx.doi.org/10.3390/solar4010003.

[10] H. Yang, F. Wang, H. Wang, J. Chang, D. Song, C. Su, Performance deterioration of p-type single crystalline silicon solar modules affected by potential induced degradation in photovoltaic power plant, Microelectron. Reliab. 72 (2017) 18–23, http://dx.doi.org/10.1016/j.microrel.2017.03.017.

[11] R. Kumar, R. Gupta, Shunts in crystalline silicon PV modules: A comprehensive review of investigation, characterization, and mitigation, Sol. Energy Mater. Sol. Cells 277 (2024) 113121, http://dx.doi.org/10.1016/j.solmat.2024.113121.

[12] R. Meena, H.M. Niyaz, R. Gupta, Investigation and differentiation of degradation modes affecting series resistance in photovoltaic cells and modules, IEEE J. Photovoltaics 13 (2) (2023) 283–290, http://dx.doi.org/10.1109/jphotov.2023.3239744.

[13] J. Pan, Z. Zou, S. Sun, Y. Su, H. Zhu, Research on output distribution modeling of photovoltaic modules based on kernel density estimation method and its application in anomaly identification, Sol. Energy 235 (2022) 1–11, http://dx.doi.org/10.1016/j.solener.2022.02.020.

[14] Y. Su, J. Pan, H. Wu, S. Sun, Z. Zou, J. Li, B. Pan, H. Zhu, Dynamic probability modeling of photovoltaic strings and its application in fault diagnosis, Energy Rep. 8 (2022) 6270–6279, http://dx.doi.org/10.1016/j.egyr.2022.04.072.

[15] E. Ortega, G. Aranguren, J. Jimeno, Determination of maximum power point with a module to module monitoring system, M3S, in: 2019 IEEE 46th Photovoltaic Specialists Conference, PVSC, IEEE, 2019, http://dx.doi.org/10.1109/pvsc40753.2019.8980935.

[16] Q. Navid, A. Hassan, A.A. Fardoun, R. Ramzan, A. Alraeesi, Fault diagnostic methodologies for utility-scale photovoltaic power plants: A state of the art review, Sustainability 13 (4) (2021) 1629, http://dx.doi.org/10.3390/su13041629.

[17] F. Spertino, A. Ciocia, P. Di Leo, R. Tommasini, I. Berardone, M. Corrado, A. Infuso, M. Paggi, A power and energy procedure in operating photovoltaic systems to quantify the losses according to the causes, Sol. Energy 118 (2015) 313–326, http://dx.doi.org/10.1016/j.solener.2015.05.033.

[18] N. Antheaume, Valuing external costs – from theory to practice: implications for full cost environmental accounting, Eur. Account. Rev. 13 (3) (2004) 443–464, http://dx.doi.org/10.1080/0963818042000216802.

[19] J. Richard, Radical Ecological Economics and Accounting to Save the Planet, Routledge, 2022, http://dx.doi.org/10.4324/9781003303121.

[20] C. Aujoux, O. Mesnil, Environmental impact assessment of guided wave-based structural health monitoring, Struct. Heal. Monit. 22 (2) (2022) 913–926, http://dx.doi.org/10.1177/14759217221088774.

[21] F.E. Alfaris, E.A. Al-Ammar, G.A. Ghazi, A.A. AL-Katheri, A cost-effective fault diagnosis and localization approach for utility-scale PV systems using limited number of sensors, Sustainability 16 (15) (2024) 6454, http://dx.doi.org/10.3390/su16156454.

[22] D. Samaniego-Rascón, M.C.G. da Silva, A.D. Ferreira, R.E. Cabanillas-Lopez, Solar energy industry workers under climate change: A risk assessment of the level of heat stress experienced by a worker based on measured data, Saf. Sci. 118 (2019) 33–47, http://dx.doi.org/10.1016/j.ssci.2019.04.042.

[23] A. Sen, A.S. Mohankar, A. Khamaj, S. Karmakar, Emerging OSH issues in installation and maintenance of floating solar photovoltaic projects and their link with sustainable development goals, Risk Manag. Heal. Policy Volume 14 (2021) 1939–1957, http://dx.doi.org/10.2147/rmhp.s304732.

[24] O. Breitenstein, J.P. Rakotoniaina, M.H. Al Rifai, M. Werner, Shunt types in crystalline silicon solar cells, Prog. Photovolt., Res. Appl. 12 (7) (2004) 529–538, http://dx.doi.org/10.1002/pip.544.

[25] O. Breitenstein, J. Bauer, J.P. Rakotoniaina, Material-induced shunts in multicrystalline silicon solar cells, Semiconductors 41 (4) (2007) 440–443, http://dx.doi.org/10.1134/s106378260704015x.

[26] K. Hasan, S.B. Yousuf, M.S.H.K. Tushar, B.K. Das, P. Das, M.S. Islam, Effects of different environmental and operational factors on the PV performance: A comprehensive review, Energy Sci. Eng. 10 (2) (2021) 656–675, http://dx.doi.org/10.1002/ese3.1043.

[27] S. Koch, D. Nieschalk, J. Berghold, S. Wendlandt, S. Krauter, P. Grunow, Potential induced degradation effects on crystalline silicon cells with various antireflective coatings, in: 27th European Photovoltaic Solar Energy Conference and Exhibition; 1985- 1990, WIP, 2012, http://dx.doi.org/10.4229/27THEUPVSEC2012-2CV.7.3.

[28] B. Li, D. Diallo, A. Migan-Dubois, C. Delpha, Performance evaluation of IEC 60891:2021 procedures for correcting I–V curves of photovoltaic modules under healthy and faulty conditions, Prog. Photovolt., Res. Appl. 31 (5) (2022) 474–493, http://dx.doi.org/10.1002/pip.3652.

[29] N. Muhammad, N.M. Ridzuan, A review of fault detection and diagnosis approaches for photovoltaic systems using voltage and current analysis, in: 2024 IEEE 4th International Conference in Power Engineering Applications, ICPEA, IEEE, 2024, pp. 25–30, http://dx.doi.org/10.1109/icpea60617.2024.10498573.

[30] C. Buerhop, D. Schlegel, M. Niess, C. Vodermayer, R. Weißmann, C. Brabec, Reliability of IR-imaging of PV-plants under operating conditions, Sol. Energy Mater. Sol. Cells 107 (2012) 154–164, http://dx.doi.org/10.1016/j.solmat.2012.07.011.

[31] C. Buerhop, T. Pickel, T. Blumberg, J. Adams, S. Wrana, M. Dalsass, C. Zetzmann, C. Camus, J. Hauch, C.J. Brabec, IR-images of PV-modules with potential induced degradation (PID) correlated to monitored string power output, in: N.G. Dhere, J.H. Wohlgemuth, K. Sakurai (Eds.), SPIE Proceedings, SPIE, 2016, http://dx.doi.org/10.1117/12.2237800.

[32] R. Kumar, V.E. Puranik, R. Gupta, Application of infrared thermography for cell-level power estimation of PID-s impacted crystalline silicon PV module, IEEE J. Photovoltaics 13 (1) (2023) 141–149, http://dx.doi.org/10.1109/jphotov.2022.3229485.

[33] R. Kumar, V.E. Puranik, R. Gupta, Unveiling the potential of infrared thermography in quantitative investigation of potential-induced degradation in crystalline silicon PV module, Sol. Energy Adv. 4 (2024) 100049, http://dx.doi.org/10.1016/j.seja.2023.100049.

[34] B. Li, A. Stokes, D.M.J. Doble, Evaluation of two-dimensional electrical properties of photovoltaic modules using bias-dependent electroluminescence, Prog. Photovolt., Res. Appl. 20 (8) (2011) 936–944, http://dx.doi.org/10.1002/pip.1161.

[35] S. Guo, E. Schneller, K.O. Davis, W.V. Schoenfeld, Quantitative analysis of crystalline silicon wafer PV modules by electroluminescence imaging, in: 2016 IEEE 43rd Photovoltaic Specialists Conference, PVSC, IEEE, 2016, http://dx.doi.org/10.1109/pvsc.2016.7750365.

[36] R. Kumar, V.E. Puranik, R. Gupta, Application of electroluminescence imaging to distinguish ohmic and non ohmic shunting in inaccessible cells within a PV module, IEEE J. Photovoltaics 14 (2) (2024) 296–304, http://dx.doi.org/10.1109/jphotov.2024.3357210.

[37] T. Kaden, K. Lammers, H.J. Möller, Power loss prognosis from thermographic images of PID affected silicon solar modules, Sol. Energy Mater. Sol. Cells 142 (2015) 24–28, http://dx.doi.org/10.1016/j.solmat.2015.05.028.

[38] J.A. Tsanakas, L. Ha, C. Buerhop, Faults and infrared thermographic diagnosis in operating c-si photovoltaic modules: A review of research and future challenges, Renew. Sustain. Energy Rev. 62 (2016) 695–709, http://dx.doi.org/10.1016/j.rser.2016.04.079.

[39] M.A. Islam, M. Hasanuzzaman, N.A. Rahim, Effect of different factors on the leakage current behavior of silicon photovoltaic modules at high voltage stress, IEEE J. Photovoltaics 8 (5) (2018) 1259–1265, http://dx.doi.org/10.1109/jphotov.2018.2841500.

[40] H.F. Barreto Miranda, L.P. da Costa, S.O. Soares, J.V. da Silva, Potential induced degradation (PID): Review, in: 2020 IEEE PES Transmission & Distribution Conference and Exhibition - Latin America, T&D LA, IEEE, 2020, http://dx.doi.org/10.1109/TDLA47668.2020.9326184.

[41] W. Luo, Y.S. Khoo, P. Hacke, V. Naumann, D. Lausch, S.P. Harvey, J.P. Singh, J. Chai, Y. Wang, A.G. Aberle, S. Ramakrishna, Potential-induced degradation in photovoltaic modules: a critical review, Energy Environ. Sci. 10 (1) (2017) 43–68, http://dx.doi.org/10.1039/c6ee02271e.

[42] W. Luo, P. Hacke, K. Terwilliger, T.S. Liang, Y. Wang, S. Ramakrishna, A.G. Aberle, Y.S. Khoo, Elucidating potential-induced degradation in bifacial PERC silicon photovoltaic modules, Prog. Photovolt., Res. Appl. 26 (10) (2018) 859–867, http://dx.doi.org/10.1002/pip.3028.

[43] C. Molto, J. Oh, F.I. Mahmood, M. Li, P. Hacke, F. Li, R. Smith, D. Colvin, M. Matam, C. DiRubio, G. Tamizhmani, H. Seigneur, Review of potential-induced degradation in bifacial photovoltaic modules, Energy Technol. 11 (4) (2023) http://dx.doi.org/10.1002/ente.202200943.

[44] M. Bertoni, D. Fenning, Defect Kinetics and Control for Module Reliability, Tech. Rep., Office of Scientific and Technical Information (OSTI), 2020, http://dx.doi.org/10.2172/1844430.

[45] D. Lausch, V. Naumann, O. Breitenstein, J. Bauer, A. Graff, J. Bagdahn, C. Hagendorf, Potential-induced degradation (PID): Introduction of a novel test approach and explanation of Increased Depletion Region recombination, IEEE J. Photovoltaics 4 (3) (2014) 834–840, http://dx.doi.org/10.1109/JPHOTOV.2014.2300238.

[46] J. Carolus, J.A. Tsanakas, A. van der Heide, E. Voroshazi, W. De Ceuninck, M. Daenen, Physics of potential-induced degradation in bifacial p-PERC solar cells, Sol. Energy Mater. Sol. Cells 200 (2019) 109950, http://dx.doi.org/10.1016/j.solmat.2019.109950.

[47] G. Badran, M. Dhimish, Field study on the severity of photovoltaic potential induced degradation, Sci. Rep. 12 (1) (2022) http://dx.doi.org/10.1038/s41598-022-26310-y.

[48] M. Dhimish, A.M. Tyrrell, Power loss and hotspot analysis for photovoltaic modules affected by potential induced degradation, Npj Mater. Degrad. 6 (1) (2022) http://dx.doi.org/10.1038/s41529-022-00221-9.

[49] R. Swanson, M. Cudzinovic, D. DeCeuster, V. V. Desai, J. Jürgens, N. Kaminar, W. Mulligan, L. Rodrigues-Barbarosa, D. Rose, D. Smith, A. Terao, K. Wilson, The surface polarization effect in high-efficiency silicon solar cells, in: 15th International PhotovoltaicScience and Engineering Conference, PVSEC-15, 2005, pp. 410–411.

[50] V. Naumann, T. Geppert, S. Großer, D. Wichmann, H.-J. Krokoszinski, M. Werner, C. Hagendorf, Potential-induced degradation at interdigitated back contact solar cells, Energy Procedia 55 (2014) 498–503, http://dx.doi.org/10.1016/j.egypro.2014.08.015.

[51] K. Sporleder, V. Naumann, J. Bauer, S. Richter, A. Hähnel, S. Großer, M. Turek, C. Hagendorf, Root cause analysis on corrosive potential-induced degradation effects at the rear side of bifacial silicon PERC solar cells, Sol. Energy Mater. Sol. Cells 201 (2019) 110062, http://dx.doi.org/10.1016/j.solmat.2019.110062.

[52] K. Sporleder, J. Bauer, B. Jäckel, V. Nauman, M. Turek, C. Hagendorf, Evolution of corrosive potential-induced degradation at the rear side of bifacial passivated emitter and rear solar cells, Phys. Status Solidi (RRL) – Rapid Res. Lett. 16 (2) (2021) http://dx.doi.org/10.1002/pssr.202100519.

[53] M.B. Koentopp, M. Krober, C. Taubitz, Toward a PID test standard: Understanding and modeling of laboratory tests and field progression, IEEE J. Photovoltaics 6 (1) (2016) 252–257, http://dx.doi.org/10.1109/JPHOTOV.2015.2487828.

[54] M. Kempe, P. Hacke, J. Morse, J. Li, Y.-C. Shen, K. Han, Electrochemical mechanisms of leakage-current in photovoltaic modules, Prog. Photovolt., Res. Appl. (2023) http://dx.doi.org/10.1002/pip.3677.

[55] V. Naumann, D. Lausch, A. Hähnel, J. Bauer, O. Breitenstein, A. Graff, M. Werner, S. Swatek, S. Großer, J. Bagdahn, C. Hagendorf, Explanation of potential-induced degradation of the shunting type by na decoration of stacking faults in Si solar cells, Sol. Energy Mater. Sol. Cells 120 (2014) 383–389, http://dx.doi.org/10.1016/j.solmat.2013.06.015.

[56] F. Martínez-Moreno, G. Figueiredo, E. Lorenzo, In-the-field PID related experiences, Sol. Energy Mater. Sol. Cells 174 (2018) 485–493, http://dx.doi.org/10.1016/j.solmat.2017.09.037.

[57] M. Ma, H. Wang, N. Xiang, P. Yun, H. Wang, Fault diagnosis of PID in crystalline silicon photovoltaic modules through I-V curve, Microelectron. Reliab. 126 (2021) 114236, http://dx.doi.org/10.1016/j.microrel.2021.114236.

[58] J. Hylský, D. Strachala, P. Vyroubal, P. Čudek, J. Vaněk, P. Vanýsek, Effect of negative potential on the extent of PID degradation in photovoltaic power plant in a real operation mode, Microelectron. Reliab. 85 (2018) 12–18, http://dx.doi.org/10.1016/j.microrel.2018.04.003.

[59] M. Kambe, K. Hara, K. Mitarai, S. Takeda, M. Fukawa, N. Ishimaru, M. Kondo, Chemically strengthened cover glass for preventing potential induced degradation of crystalline silicon solar cells, in: 2013 IEEE 39th Photovoltaic Specialists Conference, PVSC, IEEE, 2013, pp. 3500–3503, http://dx.doi.org/10.1109/pvsc.2013.6744441.

[60] X. Li, Y. Yang, K. Jiang, S. Huang, W. Zhao, Z. Li, G. Wang, A. Han, J. Yu, D. Li, F. Meng, L. Zhang, Z. Liu, W. Liu, Potential-free sodium-induced degradation of silicon heterojunction solar cells, Prog. Photovolt., Res. Appl. 31 (9) (2023) 939–948, http://dx.doi.org/10.1002/pip.3698.

[61] S. Hoffmann, M. Koehl, Effect of humidity and temperature on the potential-induced degradation, Prog. Photovolt., Res. Appl. 22 (2) (2012) 173–179, http://dx.doi.org/10.1002/pip.2238.

[62] O.K. Segbefia, A.G. Imenes, T.O. Sætre, Moisture ingress in photovoltaic modules: A review, Sol. Energy 224 (2021) 889–906, http://dx.doi.org/10.1016/j.solener.2021.06.055.

[63] O.K. Segbefia, T.O. Sætre, Investigation of the temperature sensitivity of 20-years old field-aged photovoltaic panels affected by potential induced degradation, Energies 15 (11) (2022) 3865, http://dx.doi.org/10.3390/en15113865.

[64] A. Masuda, M. Akitomi, M. Inoue, K. Okuwaki, A. Okugawa, K. Ueno, T. Yamazaki, K. Hara, Microscopic aspects of potential-induced degradation phenomena and their recovery processes for p-type crystalline Si photovoltaic modules, Curr. Appl. Phys. 16 (12) (2016) 1659–1665, http://dx.doi.org/10.1016/j.cap.2016.10.001.

[65] G.S. Huai, K. Takada, K. Ono, S. Hashimoto, N.L. Htun, F. Ohashi, N. Yoshida, Y. Sobajima, S. Nonomura, Recovery of potential-induced degraded p-type multicrystalline Si PV modules by application of a reverse DC bias, Japan. J. Appl. Phys. 61 (4) (2022) 041002, http://dx.doi.org/10.35848/1347-4065/ac52d5.

[66] S.K. Singh, N. Chander, Mid-life degradation evaluation of polycrystalline Si solar photovoltaic modules in a 100 kWp grid-tied system in east-central India, Renew. Energy 199 (2022) 351–367, http://dx.doi.org/10.1016/j.renene.2022.09.013.

[67] G.-H. Kang, H.-B. Kim, T.-H. Jung, Y. chul Ju, S.-W. Ko, H. eun Song, Prediction of the potential induced degradation of photovoltaic modules based on the leakage current flowing through glass laminated with ethylene-vinly acetate, J. Sol. Energy Eng. 137 (4) (2015) http://dx.doi.org/10.1115/1.4029933.

[68] J.M. Sancho, J. Riesco, C. Jiménez, M.d.C. de Cos, J. Montero, M. López, Atlas de Radiación Solar en España utilizando datos del SAF de Clima de EUMETSAT, Tech. Rep., Agencia Estatal de Meteorología (AEMET), 2012, URL https://www.aemet.es/es/serviciosclimaticos.

[69] J.A. Moreno Pérez, R. Muñoz Beltrán, Monthly production and open-circuit string voltage measurements after 10-year operation of three photovoltaic plants in southern Spain affected by severe potential-induced degradation [data set], 2024, http://dx.doi.org/10.5281/zenodo.11518306.